

Galactic Cepheids with *Spitzer*: II. Search for Extended Infrared Emission

P. Barmby^{1,2}, M. Marengo^{3,2}, N.R. Evans², G. Bono^{4,5}, D. Huelsman^{2,6}, K.Y.L. Su⁷, D.L. Welch⁸, G.G. Fazio²

ABSTRACT

A deep and detailed examination of 29 classical Cepheids with the *Spitzer* Space Telescope has revealed three stars with strong nearby extended emission detected in multiple bands which appears to be physically associated with the stars. RS Pup was already known to possess extended infrared emission, while the extended emission around the other two stars (S Mus and δ Cep) is newly discovered in our observations. Four other stars (GH Lup, ℓ Car, T Mon and X Cyg) show tentative evidence for extended infrared emission. An unusual elongated extended object next to SZ Tau appears to be a background or foreground object in a chance alignment with the Cepheid. The inferred mass loss rates upper limits for S Mus and δ Cep are in the range from 10^{-9} to 10^{-8} M_{\odot} yr^{-1} , with the upper limit for RS Pup as high as 10^{-6} M_{\odot} yr^{-1} . Mass loss during post-main-sequence evolution has been proposed as a resolution to the discrepancy between pulsational and dynamical masses of Cepheid variable stars: dust in the lost material would make itself known by the presence of an infrared bright nebula, or unresolved infrared excess. The observed frequency of infrared circumstellar emission ($< 24\%$) and the mass loss rate we estimate for our sources shows that dusty mass loss can only account for part of the Cepheid mass loss discrepancy. Nevertheless, our direct evidence that mass loss is active during

¹Dept. of Physics and Astronomy, University of Western Ontario, London, Ontario, N6A 3K7 Canada

²Harvard-Smithsonian Center for Astrophysics, Cambridge, MA 02138

³Dept. of Physics and Astronomy, Iowa State University, Ames, IA 50011

⁴Dept. of Physics, Università di Roma Tor Vergata, via della Ricerca Scientifica 1, 00133 Roma, Italy

⁵INAF-Osservatorio Astronomico di Roma, via Frascati 33, 00040 Monte Porzio Catone, Italy

⁶University of Cincinnati, Cincinnati, OH, 45219

⁷Steward Observatory, University of Arizona, 933 N. Cherry Avenue, Tucson, AZ 85721

⁸Dept. of Physics and Astronomy, McMaster University, Hamilton, Ontario, L8S 4M1, Canada

the Cepheid phase is an important confirmation that these processes need to be included in evolutionary and pulsation models of these stars, and should be taken into account in the calibration of the Cepheid distance scale.

Subject headings: Cepheids — infrared: stars — stars: mass loss

1. Introduction

Classical Cepheid variable stars are of key importance in the extragalactic distance scale and in studies of Galactic stellar and chemical evolution. But the very property that makes them useful as distance indicators—pulsation—also makes Cepheids difficult to model accurately. For several decades, a major problem in the understanding of Cepheids has been the discrepancy between masses estimated from stellar evolution theory and those estimated from pulsation theory (Christy 1968; Stobie 1969; Fricke et al. 1972). While the problem was partly addressed by revision of radiative opacities and changes in evolutionary tracks (Moskalik et al. 1992), the discrepancy persists at the 10–20% level (Caputo et al. 2005; Keller & Wood 2006). Measurements of several Cepheid masses are now available from binary systems (Benedict et al. 2007; Evans et al. 2008, 2009), but the comparison with evolutionary and pulsational masses has not yet produced a definitive result.

There are a number of possible solutions to the ‘Cepheid mass discrepancy,’ summarized by Bono et al. (2006). Recent studies have come to differing conclusions on which might be responsible: Caputo et al. (2005) suggested that mass loss can account for the discrepancy, while Keller (2008) concluded that additional mixing in Cepheid main sequence progenitors was responsible. Mass loss remains one of the less-understood parameters in stellar evolutionary theory (Willson et al. 2008; Vink 2008), and its relevance to Cepheid masses is still not completely clear. In the last several years, several lines of investigation have suggested that mass loss may be important in Cepheids. These include the discovery of extended near-infrared emission from a number of Galactic Cepheids (Mérand et al. 2006, 2007; Kervella et al. 2006), possibly from circumstellar shells, as well as theoretical modeling of pulsation-driven mass loss (Neilson & Lester 2008) and its application to Magellanic Cloud Cepheids (Neilson et al. 2009, 2010). Both the presence of shells around nearby Cepheids and the evidence for infrared excess in LMC Cepheids have implications for the stars’ derived diameters and therefore for the distance scale. Systematic effects on distances are possible, if Cepheid mass-loss is substantial enough to affect spectral energy distributions, and if it works differently in nearby and distant galaxies (e.g., is a function of metallicity). Neilson et al. (2010) concluded that mass loss in Cepheids “has an important effect on the structure of the IR P-L [infrared period-luminosity] relations” although the extent of the

effect is not well characterized.

Attempts to estimate Cepheid mass-loss rates through infrared observations began about 25 years ago. McAlary & Welch (1986) used infrared excesses inferred from the IRAS Point Source Catalog to estimate mass loss rates of $\dot{M} < 10^{-9} - 10^{-8} M_{\odot} \text{ yr}^{-1}$, while Deasy (1988) combined ultraviolet and infrared observations to estimate upper limits of $\dot{M} < 10^{-10} - 10^{-7} M_{\odot} \text{ yr}^{-1}$. Welch & Duric (1988) used radio observations to place similar upper limits on the mass loss in ionized gas. In general these rates are too low to account for the mass discrepancy. Recently, the *Spitzer Space Telescope* has been used in a number of studies of Cepheids in the mid-infrared, including the period-luminosity relation (Ngeow & Kanbur 2008; Freedman et al. 2008; Marengo et al. 2010a). Kervella et al. (2009) combined ground-based infrared imaging and interferometric measurements with *Spitzer* data (including data from the program described here) to detect compact circumstellar envelopes around both ℓ Car and RS Pup; the latter was previously known to be associated with a reflection nebula.

To investigate the possibility of infrared excesses due to mass loss, we have obtained *Spitzer* (Werner et al. 2004) observations of a sample of 29 Classical Cepheids. Our results on the mid-infrared period-luminosity and period-color relations for Cepheids are presented in Marengo et al. (2010a, Paper I); a detailed analysis of extended emission near δ Cep is presented by Marengo et al. (2010b). In Paper I we determined that there was no evidence from IRAC colors for warm circumstellar dust. The present paper investigates the presence of cooler dust around this sample of Cepheids via a search for extended mid-infrared emission. An important consideration is that extended emission may be the result of recent star-forming activity near a Cepheid rather than mass loss from the Cepheid itself. However, distinguishing those two different causes is not straightforward, so a search for extended emission places an upper limit on the amount of mass loss. Except where mentioned otherwise, in all of the following analysis we use the stellar distances given by Fouqué et al. (2007).

2. Observational data

The sample selection and first-epoch observations are described in detail by Marengo et al. (2010a). Briefly, 29 Galactic Cepheid variables and 3 non-variable supergiants were observed with both IRAC (Fazio et al. 2004) and MIPS (Rieke et al. 2004) as part of *Spitzer* Space Telescope General Observer, program ID 30666. The IRAC observations described by Marengo et al. (2010a) were primarily made in subarray mode. The 6 brightest stars were observed in full-array mode so that fluxes could be measured by fitting the outer part of the point spread function (PSF); 4 stars were observed in both full-array and subarray modes. The MIPS observations used the Photometry Astronomical Observing Template with the

shortest possible observation time (48.2 s) at 24 μm and varying times (37.7–1300.2 s) at 70 μm . Three stars (S Nor, V Cen, U Sgr) were observed in two adjacent fields of view at 70 μm to better cover the surrounding clusters. While our target SZ Tau (see §3.5) may also be in the cluster NGC 1647 (Turner 1992), after inspecting its 24 μm image, we changed the planned 70 μm observation to use only one field of view centered on the star. This allowed us to increase the observation time and, as a bonus, also provided a second epoch of 24 μm observations. We performed simple aperture photometry on post-BCD mosaics primarily from the pipeline version S16.1 output. For the three cluster stars, the 70 μm data were remosaiced using MOPEX to combine the data for the two fields of view. For two stars (RS Pup, GH Lup) the 70 μm mosaics were remade to remove negative sidelobes.

2.1. New IRAC data and reduction

To follow-up earlier results, we obtained some additional *Spitzer* data in Cycle 5, on the dates 2008 October 5–6. All stars were observed in full-array mode with IRAC as part of Guaranteed Time program 50350 (PI G. Fazio). This increased the field of view for stars which had previously been observed only in subarray mode, and also provided deeper observations (2-second frames at each of 36 dither positions) for all stars. Each target fainter than $K = 2$ was observed with the IRAC full frame 12 second High Dynamic Range (HDR) mode, using a 12 point Reuleaux small scale dither pattern for a total integration time of 144 sec in each band. HDR 12 second frames were used to better reveal the area closer to the saturated cores of the targets, which also helped the PSF subtraction process. For the six brightest sources, in order to avoid excess saturation, targets were observed with 2 second frames using IRAC full frame non-HDR mode and the 36 point Reuleaux small scale dither pattern, for a total integration time of 72 s in each band. The Reuleaux dither pattern was used to achieve the required total exposure time while obtaining the best possible spatial sampling of the targets in anticipation of the PSF subtraction process.

The basic calibrated data (BCD) for all observations were reduced using the custom post-BCD software IRACproc (Schuster et al. 2006), which generated mosaics for each source with the final exposure depth and outliers removed. The final images had a pixel scale of 0.8627 arcsec pix^{-1} ($1/\sqrt{2}$ the original IRAC pixel scale) which provides a better sampling of the sources' PSF for a more accurate PSF subtraction. The PSF subtraction was also performed using a routine part of IRACproc, which has been extensively tested in other *Spitzer* programs (Marengo et al. 2006, 2010a; Luhman et al. 2007) to search for faint structures and point sources around bright stars.

2.2. MIPS photometry

Although the MIPS observations used in this paper are the same as those in Marengo et al. (2010a), a major purpose of the present work is to examine extended emission around a subset of the stars in our sample. Accordingly, we have performed point source fitting and subtraction on the $24\ \mu\text{m}$ images of some targets to separate the contributions of the star and extended emission to the total flux density. The data were reprocessed with the MIPS instrument team Data Analysis Tool using standard procedures. The PSF used for the $24\ \mu\text{m}$ subtraction was built from the observations of the A4 V star, τ_3 Eri (Su et al. 2008), which matches well with the theoretical PSF computed from STinyTim Program (Krist 2006) after proper smoothing. The subtraction was done by iteratively shifting the PSF to match the centroid of the target in sub-pixel accuracy, adjusting its scaling, and subtracting it from the target image until the residual inside $r < 12''$ (\sim to the first bright Airy ring of the PSF) was minimized. The residual flux is generally less than 1% of the total flux of a typical point source on a clean background.

To estimate the non-point source emission near stars showing extended emission in the MIPS bands, we used the results of point source fitting and subtraction. We performed aperture photometry of the point and extended emission on images which had the field (but not the target) stars subtracted, using the largest apertures which could be contained in the image. From this we subtracted the flux measured by fitting and subtracting the target stars to derive the total non-point source emission. This procedure depends on accurate background subtraction for the large-aperture photometry, particularly difficult in the $70\ \mu\text{m}$ images, and the resulting uncertainties are large. An alternative approach which can constrain the physical conditions within regions of extended emission is used by Marengo et al. (2010b): measuring the surface brightness of the extended emission in small areas. Because the stars are heavily saturated in the IRAC bands, this is the only method available to investigate the extended emission visible in the IRAC images. In both IRAC and MIPS images we measured the surface brightness in several small regions near stars with extended emission, and subtracted backgrounds measured in regions located off the extended emission. The regions used are shown in the images of the relevant stars; the measured surface brightnesses are reported in Table 1.

3. Analysis

Infrared colors were used in Paper I to demonstrate a lack of warm circumstellar dust in our sample of Cepheids. However, dust mass lost from Cepheids and then transported to larger distances would be expected to be cooler, and possibly visible as extended infrared

emission. One example of this phenomenon is the infrared nebula visible around δ Cep (Marengo et al. 2010b): here we complete the survey of our Cepheid and comparison star sample. None of the stars showed any extended emission in the $3.6 \mu\text{m}$ or $4.5 \mu\text{m}$ bands, so those bands are not discussed further here. Distinguishing between extended emission associated with a specific star and that due to nearby Galactic cirrus and/or star formation, especially at low Galactic latitudes, is not always straightforward. We expect that emission associated with an individual star should be centered on or near the star, with its surface brightness decreasing with increasing distance from the star. Unrelated infrared emission will not in general have these characteristics, although of course it could hide or confuse real low level emission. For brevity, we refer to unrelated infrared emission as ‘cirrus’ below, although we recognize that it may not be true Galactic cirrus emission.

Of our sample of 29 Cepheids, 16 showed clear signs of cirrus in the IRAC $8 \mu\text{m}$ images: AQ Pup, BF Oph, DT Cyg, FF Aql, GH Lup, RS Pup, S Mus, S Nor, SW Vel, T Mon, U Car, U Sgr, V636 Sco, V Cen, VY Car, and X Cyg. Cirrus is also visible in the MIPS images of GH Lup, V Cen, VY Car and U Sgr.¹ As expected, the presence of cirrus is related to Galactic latitude: of the Cepheids in our sample with $|b| < 10^\circ$, 15 of 23 appear to be surrounded by cirrus emission. The remaining star with apparent unrelated emission is DT Cyg, at $b = -10.8^\circ$. The list of cirrus sources include three of the four stars we believed as cluster members (S Nor, V Cen, U Sgr); this classification is confirmed by Gieren et al. (1997), who also found that VY Car is a member of the Car OB 2 association. The extended emission near these stars could be associated with either their clusters or the general interstellar medium. Figure 1 shows some examples of stars surrounded by cirrus.

As a quantitative test for excess infrared emission near the stars, we computed the average surface brightness around each star and compared it to a background measurement. The IRAC $8 \mu\text{m}$ images were used for this measurement as they have a larger uniform-exposure field of view than the MIPS images, and much better sensitivity to extended emission than the $5.8 \mu\text{m}$ images. The average surface brightnesses were measured in 1 arcminute radius apertures surrounding each star, with the PSF subtraction residuals and bright star artifacts masked. The background measurement was made in an annulus with inner and outer radii of 74 and 98 arcseconds. Point sources near the target stars, imperfect PSF subtraction, and unrelated cirrus emission all complicate the comparison between low-surface-brightness emission near the stars and in their vicinities. To be conservative, we consider as having possible extended infrared emission only those stars for which the average surface brightness in the measurement aperture exceeds that in the background aperture by 20 times the

¹Of our three non-variable comparison stars, HD 1822296 and HD 183864 were observed in subarray mode only; ψ And was observed in full-array mode and shows no evidence for cirrus.

quadrature sum of the surface brightness standard deviations. Since our measurement errors are influenced by the factors listed above and are unlikely to be Gaussian, we do not consider these detections to have true 20σ significance—the value chosen is intended as a starting point to guide the analysis.

We found no evidence for extended infrared emission around two stars which have been previously found to have circumstellar envelopes: Polaris (Mérand et al. 2006) and Y Oph (Mérand et al. 2007).² Other stars with neither cirrus or extended infrared emission are BB Sgr, U Aql, V350 Sgr, W Sgr, β Dor, η Aql and ζ Gem. Five stars showed both cirrus and extended emission centered on or near the star: GH Lup, RS Pup, S Mus, T Mon, and X Cyg. Three further stars had little detectable cirrus but did have extended infrared emission centered on the star: δ Cep, ℓ Car, and SZ Tau.

The extended emission around δ Cep is discussed in detail by Marengo et al. (2010b) and briefly summarized here. The emission consists of a large-scale (0.1 pc) arched structure visible at $70\ \mu\text{m}$, with diffuse, filamentary emission at 5.8, 8.0 and $24\ \mu\text{m}$ contained within the arch. The brightest region of this diffuse emission is between δ Cep and its hot companion HD 213307. The symmetry axis of the $70\ \mu\text{m}$ emission near δ Cep is aligned with the star’s velocity vector relative to the local ISM, suggesting a bow-shock at least partly swept-up from the ISM. The emission near the stars is hypothesized to be due to the interaction of their stellar winds. The mass loss rates required for the creation of these structures are estimated to be in the range $5 \times 10^{-9} - 6 \times 10^{-8}\ M_{\odot}\ \text{yr}^{-1}$.

The remaining stars with extended infrared emission are discussed individually below.

3.1. GH Lup

Images of GH Lup are shown in Figure 2. The most obvious component of extended emission is an arc-like structure to the east of the star, visible at 8, 24, and $70\ \mu\text{m}$. The structure is not centered on the star itself but roughly $20''$ to the south (2.2×10^4 AU at the star’s distance) with a radius of approximately $32''$ (3.6×10^4 AU). Spatially coincident with the arc is a point source visible at 5.8 and $8.0\ \mu\text{m}$ only, which we can identify with the $K_s = 9.5$ object 2MASS J15244147-5251282. Because the region is crowded, with copious diffuse emission, it is unclear whether the arc near GH Lup is related to the Cepheid, the nearby star, or neither. The stellar crowding also makes defining regions for surface

²The extended emission found by those authors was at very small spatial scales (a few stellar radii), well below our angular resolution.

photometry of the diffuse emission difficult; we chose the regions marked in Figure 2 to avoid stars in the 8 μm image and capture at least some of the extended emission. The resulting measurements are given in Table 1, with the colors of the extended emission plotted in Figure 3. Using a modified blackbody spectrum to assign color temperatures from the S_{24}/S_{70} ratios yields $55 < T < 81$ K, depending on the emissivity index β for the modified blackbody. The S_8/S_{24} ratios for GH Lup tend to be higher than those found for the other stars with extended emission. Together with the structure of the emission and the extensive nearby cirrus, this leads us to speculate that the emission near GH Lup is only moderately likely to be associated with the star itself (see §4).

3.2. ℓ Car

Images of ℓ Car are shown in Figure 4. These data were also analyzed by Kervella et al. (2009), who failed to detect any nebulosity in the *Spitzer* images, but found evidence of small scale ($\sim 1''$) extended emission in near- and mid-IR interferometric data, attributed to hot circumstellar dust. Our PSF-subtracted IRAC images show low surface brightness emission, at 5.8 and 8.0 μm , surrounding the star with a radius of $\sim 35''$, or 1.7×10^4 AU at a distance of 498 pc (Kervella et al. 2009). We do not detect any significant extended emission at 70 μm , and only a tentative excess at 24 μm , northeast of the nearly saturated core of the PSF-subtracted star. The 8.0 μm emission appears brighter northwest of the star, where an arc-like structure is detected at a distance of $\sim 30''$ (1.5×10^4 AU). Following a suggestion by the referee, we computed the components of the star’s Galactic peculiar space motion and their projection onto the sky, using the procedure described by Marengo et al. (2010b). The star’s position and proper motion were taken from the Hipparcos catalog (Perryman et al. 1997), the distance from Kervella et al. (2009), and heliocentric radial velocity of 3.6 km s^{-1} from Nardetto et al. (2009). We find a space velocity of 24.9 km s^{-1} along a position angle of 315° (east of north), with the direction shown as an arrow in the second panel of Figure 4. The vector is roughly aligned along the direction from the star to the arc-like structure, suggesting a possible connection between the two (e.g., a bow shock, reflection nebula, or light echo). Image artifacts from the PSF subtraction and the star make the connection difficult to secure, however. Artifacts also make it impossible to accurately measure the surface brightness of the extended emission, and thus estimate the mass loss rates that could be responsible for the observed nebulosity. Higher spatial-resolution imaging covering a wider area would clearly be useful in further study of ℓ Car.

3.3. RS Pup

RS Pup is embedded in a well-known reflection nebula (Westerlund 1961; Havlen 1972) whose infrared emission has been noted by numerous authors (e.g., Gehrz 1972; McAlary & Welch 1986). PSF-subtracted images of RS Pup are shown in Figure 5. The morphology of the extended infrared emission varies with wavelength but the brightest region is to the north-east of the star. Most of the emission is within about $80''$ of the star, a linear distance of 0.77 pc at the 1.992 kpc distance of RS Pup (Kervella et al. 2008), although the small field of view of the $70\ \mu\text{m}$ image makes this difficult to pin down. The MIPS data, but not the full-frame IRAC data, were also analyzed by Kervella et al. (2009), so here we present the first image of the resolved $8.0\ \mu\text{m}$ emission around RS Pup. Kervella et al. (2009) attributed the $\gtrsim 20\ \mu\text{m}$ resolved emission, as well as the infrared excess in the IRAS data, to an extended envelope with a radius of roughly 1 pc and a temperature of ~ 40 K. Kervella et al. (2009) also detected resolved emission at much smaller angular distances to the star, and attributed this to a “warm and compact component” at a distance of 300–3000 AU and a temperature of a few hundred K. They proposed that the warm component comes from RS Pup’s mass loss, and the cold component is interstellar medium gas compressed by the star’s stellar wind. In Marengo et al. (2010b) a similar origin for the extended infrared emission around δ Cep was proposed.

We add to the analysis of RS Pup’s extended emission by examining the colors of the extended emission. Using the surface brightness measurements in Table 1, Figure 3 plots the ratios of the extended emission around RS Pup and S Mus, with the values derived for δ Cep by Marengo et al. (2010b) for comparison. Using a modified blackbody spectrum to assign color temperatures from the S_{24}/S_{70} ratios yields $50 < T < 80$ K, depending on the emissivity index β for the modified blackbody. These temperatures are a little lower than the values derived for δ Cep; however, compared to δ Cep, the RS Pup nebulosity is more distant from the central star. Like the δ Cep nebulosity, the RS Pup extended emission has $S_{8.0}/S_{24} \sim 0.5$, suggesting that some polycyclic aromatic hydrocarbons (PAHs) must be present (pure dust at $50 < T < 80$ K would imply a much lower ratio; Marengo et al. 2010b). We can also compute an average dust temperature for the RS Pup nebulosity using the total flux densities of the extended emission. At $70\ \mu\text{m}$ we used the largest aperture that will fit on the image ($85''$ radius) to derive a total flux density of 9.7 Jy. At $24\ \mu\text{m}$ we measured the flux density in a large aperture ($72''$ radius) and subtracted the PSF-fitting flux of the central source to derive an extended emission flux density of $(620 - 330 =) 290$ mJy. Using a modified blackbody spectrum to assign color temperatures from the ratio of the two bands yields $44 < T < 57$ K, depending on β . These temperatures are a little higher than the estimate of 40 K given by Kervella et al. (2009), who extrapolated the $70\ \mu\text{m}$ surface brightness profile to derive a larger total flux density.

The dust mass in the RS Pup nebula is best estimated with far-infrared photometry, since as Figure 5 shows, the stellar emission is insignificant at wavelengths of $70 \mu\text{m}$ and beyond. Because our $70 \mu\text{m}$ MIPS images have a rather small field of view, the difficulty of accurate background subtraction makes any attempt to estimate the total flux density (including that of Kervella et al. 2009) problematic. However, a rough estimate of total dust mass is possible and provides a comparison point for previous results. We use the formula given in Eq. 2 of Evans et al. (2003), assuming that all of the $70 \mu\text{m}$ emission is from optically thin dust with $T = 40 - 80 \text{ K}$ and emissivity $\kappa_\nu = 3Q_\nu/\rho a$ in $\text{cm}^2 \text{ g}^{-1}$. For comparison with McAlary & Welch (1986), we use $\kappa = 19.0$, scaled from the $100 \mu\text{m}$ value the $a = 0.1 \mu\text{m}$ ‘dirty silicate’ dust model in Jones & Merrill (1976) via a $Q_\nu \propto \lambda^{-2}$ wavelength dependence. The derived total dust masses for RS Pup are in the range $1 \times 10^{-3} - 1.4 \times 10^{-2} M_\odot$. (The range of values here accounts for the change in the Planck function, but not any temperature dependence of the dust emissivity, over the given temperature range.) The uncertainty due to temperature is compounded by the uncertainty in dust emissivity: for example, using the wavelength-dependent emissivity of amorphous fayalite given by Evans et al. (2003) would result in a value of κ nearly 15 times larger (and thus masses 15 times smaller) than given above. The $100 \mu\text{m}$ flux density from the IRAS Small Scale Structure Catalog (Helou & Walker 1988) should provide a better estimate of the total flux density of the RS Pup nebula. Using this measurement, McAlary & Welch (1986) estimated a total dust mass of $0.028 M_\odot$ (for their adopted distance of 1.778 kpc), or $0.035 M_\odot$ for the 1.992 kpc distance we use. The mass derived from the $70 \mu\text{m}$ flux density is the same order of magnitude, likely smaller because our observations do not capture the full extent of the RS Pup nebula.

As McAlary & Welch (1986) point out, the large size of the RS Pup nebula makes estimating a mass-loss rate from the nebular mass “extremely difficult”. With a gas-to-dust ratio of 100, the McAlary & Welch (1986) dust mass converts to a total mass of $3 M_\odot$. An argument in favor of the idea that some of the nebula is swept-up interstellar medium (ISM) results from a simple comparison of the nebula mass with the helium-burning timescale of RS Pup (Kervella et al. 2009). Taking the mass estimate for RS Pup provided by Caputo et al. (2005), the helium burning time inside the instability strip is of the order of 1.2 Myr . If all of the nebula consists of mass lost by RS Pup during its helium-burning phase, the implied mass-loss rate would be $\gtrsim 10^{-6} M_\odot \text{ yr}^{-1}$. This would imply a total mass loss at least of the order of 10% . As Kervella et al. (2009) note, this would be sufficient to solve the pulsational/evolutionary mass difference for RS Pup. However, as noted by Neilson & Lester (2008), the observational mass loss rate for RS Pup disagrees with their theoretical predictions ($1.6 - 6.5 \times 10^{-9} M_\odot \text{ yr}^{-1}$) by several orders of magnitude. These predictions do appear to fit the observational data for Magellanic Cloud Cepheids (Neilson et al. 2009, 2010), which

makes it more believable that at least some of the mass in the RS Pup nebula did not originally belong to the star. The observed $S_{8.0}/S_{24}$ ratio is too high for pure dust emission, but lower than typical for the typical PAH content of the ISM. Since Cepheid atmospheres are oxygen-rich and not expected to form PAHs, this suggests that both swept-up ISM (or pre-existing material containing PAHs) and stellar wind must comprise the nebula.

3.4. S Mus

Images of S Mus are shown in Figure 6. There are slightly extended emission features to both the north and south of the star visible at both 8 and 24 μm , with radial extents 35–45'' ($2.9 - 3.7 \times 10^4$ AU at a distance of 820 pc). There is also extended emission visible at 70 μm , to a radius of about 55'' (4.5×10^4 AU), although the morphology is different at that wavelength. The surface brightness of this emission is faint compared to that around RS Pup, and the orientation of the PSF subtraction residuals makes computing $S_{8.0}/S_{24}$ and S_{24}/S_{70} at the same location difficult. The S Mus point shown in Figure 3 is for the box marked ‘3’ in the IRAC images and ‘2’ in the MIPS images. Although uncertain, the colors imply an even lower PAH content than in RS Pup and δ Cep, and a somewhat higher color temperature (70–120 K). This star has a high-temperature companion (Evans et al. 2006) and the extended emission could be associated with that star rather than S Mus itself, or the companion could be responsible for heating the circumstellar material (as hypothesized for δ Cep; Marengo et al. 2010b).

The photometry of the extended emission around S Mus can be used to estimate the mass lost by the star. Large-aperture (35'' radius) photometry of the 70 μm emission yields a total flux density of 96 ± 12 mJy; subtracting the point-source flux density (measured in a 16'' radius aperture as for Paper I) of 39 ± 11 mJy yields a nebular flux density of 57 ± 16 mJy. We use the same dust mass estimation procedure as for RS Pup, a temperatures of 70–120 K, and a stellar distance of 0.88 kpc to derive an implied dust mass $4 - 17 \times 10^{-7} M_{\odot}$. With a gas-to-dust ratio of 100, the total implied mass would be approximately $4 - 17 \times 10^{-5} M_{\odot}$. If we instead use $\kappa = 56$ as in Marengo et al. (2010b), the total mass agrees quite well with that derived δ Cep. Given the photometric uncertainties, the agreement may well be coincidental; however the order of magnitude comparison is intriguing. A mass loss timescale can be estimated by dividing the distance to the emission (35'' is 0.15 pc at the distance of S Mus) by the escape velocity (100 km s $^{-1}$) to yield $t \approx 1500$ yr, so the resulting mass loss rate would be $3 - 10 \times 10^{-8} M_{\odot} \text{ yr}^{-1}$. As for δ Cep, this estimate is consistent with the predictions of Deasy (1988) but well above those of Neilson & Lester (2008). There are two reasons why our value for the mass loss rate is likely to be an upper limit, and therefore

larger than the Neilson & Lester (2008) predictions. (1) We assumed that all of the dust responsible for the extended emission comes from wind material as opposed to having been swept-up from the ISM; as for RS Pup, the PAH content implies that ISM sweeping is likely relevant. (2) Using the escape velocity to estimate the nebula’s age results in the minimum possible age, and hence a maximum for the mass loss rate.

We can estimate the total mass lost for S Mus through its mass and crossing time for the instability strip, as above for RS Pup. We estimated pulsational and evolutionary masses through the relation provided by Caputo et al. (2005, Tables 2–5); using the near-infrared photometry from Laney & Stobie (1994, transformed to the 2MASS system using Koen et al. 2007) and optical photometry from Pedicelli et al. (2010), corrected for extinction using the reddening given by Fernie et al. (1995) and the reddening law of Cardelli et al. (1989). We used an intrinsic distance based on the near-infrared photometry and period-Wesenheit relations provided by Persson et al. (2004). This procedure results in a mean mass $7.0 \pm 1.5 M_{\odot}$, and according to Bono et al. (2000) the corresponding crossing time of the instability strip is of the order of 0.14 Myr. Given the mass loss rate above, this results in a small total mass loss of $0.006 M_{\odot}$. Using the recent estimate of the radius of S Mus by Groenewegen (2008) and the period-mass-radius relation given by Bono et al. (2001), the pulsation mass is lower, $\sim 5 M_{\odot}$, and the instability strip crossing time much longer, of order 1 Myr; however the total mass lost would still be only $0.04 M_{\odot}$, too small to significantly affect the mass discrepancy.

3.5. SZ Tau

SZ Tau was the only Cepheid found in Paper I to have a statistically significant $[24] - [70]$ color excess. Images of this star are shown in Figure 7. There is an extended object about $25'' \times 8''$ clearly visible in the PSF-subtracted $8.0 \mu\text{m}$ image, about $7''$ to the north-east of the star. At the 512 pc distance to the star, $25'' \times 8''$ corresponds to linear scales of $(1.3 \times 0.4) \times 10^4$ AU. The object is not clearly visible in the $5.8 \mu\text{m}$ band, due to PSF subtraction residuals, however it is visible at $24 \mu\text{m}$ and appears to be the source of most of the $70 \mu\text{m}$ luminosity. The object is resolved at $24 \mu\text{m}$ and has a similar appearance in two images in that band taken about a year apart, suggesting that it is not an instrumental artifact or a solar system object. Noriega-Crespo et al. (1997) detected a “ridge or filament” of similar shape but much larger angular size in IRAS imaging of Betelgeuse; they suggested that this structure is emission from the interstellar medium, unrelated to the star. Turner (1992) concluded that SZ Tau is a first-overtone pulsator and noted several other unusual characteristics of this star (e.g., period changes), but it is unclear how these features could

be related to the presence of extended emission.

The elongated shape of the emission near SZ Tau suggests a background galaxy. The infrared colors should yield further information on the object’s nature, although photometry of the SZ Tau extended emission is complicated by the star itself. At $70\ \mu\text{m}$, the extended emission appears to be the dominant source of emission. When we measure flux density in a $35''$ radius aperture centered on the $70\ \mu\text{m}$ peak and a $39\text{--}65''$ background annulus, the resulting flux density (which may include some contribution from the star) is $74\ \text{mJy}$.³ We measured the flux density of the SZ Tau extended emission at $24\ \mu\text{m}$ by doing a large-aperture ($35''$ radius) measurement on the extended emission+star and subtracting the PSF-fitting star flux, to give an extended emission flux density of $(175 - 144 =) 31\ \text{mJy}$. Measuring the $8\ \mu\text{m}$ flux density is the most difficult since there is significant contamination from the PSF subtraction residuals. Measuring the emission on an image with the residuals masked in $35''$ radius aperture with $35\text{--}43''$ background annulus gives a flux density of $10\ \text{mJy}$; applying the IRAC extended source photometric correction changes this to $7.4\ \text{mJy}$. Different approaches to residual masking and photometric aperture change the resulting flux density by $\sim 20 - 30\%$, so the value is highly uncertain. This is hardly surprising since the extended emission is more than 100 times fainter than the star at $8\ \mu\text{m}$. Consistent with this result is the classification of the star’s mid-infrared spectrum as normal, with no dust, based on data from the PHT-S instrument on the Infrared Space Observatory (Hodge et al. 2004).

We can ask whether the the galaxy-like appearance of the extended emission near SZ Tau is consistent with its mid-infrared flux densities and colors. The object is rather bright for a galaxy: number counts at $24\ \mu\text{m}$ (Shupe et al. 2008) show that there are only $3.5\text{--}4$ galaxies per square degree brighter than about $15\ \text{mJy}$. Taken together, all of our $24\ \mu\text{m}$ Cepheid images cover about 0.5 square degree, so we might expect 1 or 2 such galaxies in our survey. Figure 8 compares the colors of the SZ Tau extended emission with some comparison samples. The color $f_{8.0}/f_{24} = 0.24$ is consistent with the colors of both nearby and distant galaxies (Muñoz-Mateos et al. 2009; Hainline et al. 2009). However, the flux ratio $f_{24}/f_{70} = 0.42$, while inconsistent with an unobscured stellar source, is rather high for a galaxy detected at $70\ \mu\text{m}$; such galaxies typically have $0.05 \lesssim f_{24}/f_{70} \lesssim 0.11$ (Frayser et al. 2006). The flux ratios and colors are more consistent with those of candidate young stellar objects detected in the Cepheus Flare (Kirk et al. 2009), although YSOs do not typically have lenticular morphologies. Planetary nebulae can have asymmetric shapes, but the SZ Tau emission has quite different colors (see Figure 8). The best candidates to explain the

³The flux density for this star reported in Marengo et al. (2010a) is slightly different because that value was measured centered on the $24\ \mu\text{m}$ star position. Also, there is a bright far-infrared source about $80''$ to the northwest of the star’s position which may also contaminate the photometry.

extended emission near SZ Tau are either an unusually-shaped Galactic object (possibly a YSO) or a background galaxy with very weak cold dust emission. This mysterious object warrants further investigation. A more definitive conclusion on its nature could be reached with higher spatial resolution infrared observations, in which the flux from the star and extended emission were more clearly separated.

3.6. T Mon and X Cyg

These stars show extended emission in the IRAC 8.0 μm band with only tentative detections in the MIPS bands; images can be seen in Figures 9 and 10. In the image of T Mon, there appears to be cirrus across the entire field of view. However, there is brighter nebulosity closer to the star, specifically to the north and south in an hourglass-like shape extending to about $45''$ radius (6.2×10^4 AU, or 0.3 pc, at a distance of 1389 pc). The emission is centered around the star, suggesting that it may be locally illuminated. The extended emission near X Cyg has the second-lowest significance (after GH Lup) of the stars with emission above background levels. It is brightest to the northwest of the star and concentrated within a radius of $30''$ (3.5×10^4 AU, or 0.16 pc, at a distance of 1163 pc). For both stars, the 24 μm images show hints of enhanced brightness at similar positions to the 8 μm emission, but these positions are too close to the PSF subtraction residuals to make definitive conclusions, or to measure a surface brightness. There is no corresponding detectable emission at 70 μm . With both stars having extended emission observed at only one wavelength, the detections must be regarded as tentative. Observations with the James Webb Space Telescope, particularly its coronagraphs, would provide an avenue to confirm or refute them. If the detections are confirmed, the properties of these stars may provide a challenge in relating them to any mass loss. Neilson & Lester (2008) predicted that mass loss rates, while showing large scatter with period, are generally larger for long-period stars. T Mon is a long period star with a companion (Evans et al. 1999), while X Cyg has a period of 16.4 d and no known companion hotter than type A5 (Evans 1992). However, a low-mass companion with an orbit in the plane of the sky is not ruled out for X Cyg and might be important in forming and/or shaping an extended nebula.

4. Discussion and Conclusions

Spitzer mid-infrared observations of Cepheids have produced no strong evidence for large amounts of warm circumstellar dust (Marengo et al. 2010a). Here we use the same observations to place limits on cooler dust. Of our sample of 29 Cepheids, two stars (RS Pup

and δ Cep) have well-detected extended infrared emission, two (GH Lup and S Mus) have possible extended emission at 24 and 70 μm , and a further three (ℓ Car, T Mon and X Cyg) show tentative evidence for extended infrared emission at shorter infrared wavelengths only.

Is there anything particularly special about the stars in which we do have (tentative) evidence for mass loss? Our observations of the nebulosity around δ Cep and S Mus suggest that the detectability of a dustless wind might be enhanced when interstellar matter around the Cepheid is swept up into a bow shock, and a hot companion heats the material. Compared to the emission around RS Pup and GH Lup, the S_{24}/S_{70} ratio (a proxy for dust temperature) is higher near S Mus and δ Cep. Both of these stars have known hot companions, while RS Pup and GH Lup do not (although low-temperature companions cannot be excluded using current data). A counter example might be provided by T Mon, which also has a hot companion, but does not have detectable extended emission at 24 or 70 μm or an infrared excess; however, T Mon’s companion is cooler (type A0) than that of the other two stars (B3 and B7-8).

The surface brightness ratios $S_{8.0}/S_{24}$ are a rather crude tool for deriving detailed physical conditions, but can give some insight into the PAH content of the ISM near these stars. The low PAH content indicated by the $S_{8.0}/S_{24}$ ratios for RS Pup, S Mus and δ Cep—much lower than in the NGC 7023 reflection nebula, or the ISM in general—suggests that the ISM around these stars has been diluted to some extent by the stellar winds. The higher PAH content near GH Lup would imply less dilution, suggesting that the emission there may be unrelated to the star. We caution that, while the amount of dilution might be indicated by the $S_{8.0}/S_{24}$ ratio, high spatial-resolution spectroscopy in which the stellar and extended emission are separated would provide much greater physical insight into the conditions near these stars.

The IRAC-only extended emission near ℓ Car, T Mon, and X Cyg also suggests that these stars are somehow unusual. However, we have been unable to find any clear distinction between these stars and the three which also show extended MIPS emission, or between all seven stars and our full Cepheid sample. Like RS Pup, ℓ Car and T Mon have long periods (> 27 d) and low temperatures; GH Lup, S Mus and δ Cep have periods < 10 d, and X Cyg is intermediate with a period of 16.4 d. Six of the seven stars have super-solar metallicity (Romaniello et al. 2008; Andrievsky et al. 2005; Kovtyukh et al. 2005) but the difference in mean metallicity between these stars and the other stars in the sample is barely statistically significant ($p = 0.025$). Evans (1992) placed strong limits on the presence of hot companions in Cepheids: of the stars in our sample, 3 of the 7 with possible extended emission have such companions (S Mus, δ Cep, T Mon), as do 5 of the 22 stars without extended emission (an additional 3/23 are radial-velocity binaries). With such small numbers it is not yet possible

to say whether the presence of hot companions enhances the detection of extended infrared emission.

RS Pup is clearly different from all of the other Cepheids in our sample in terms of the extent and brightness of its infrared emission. One possible explanation is that this star has swept up more material, either by having been on the instability strip for longer (unlikely, since long-period stars evolve faster) or by being located in a region of higher density in the interstellar medium. An alternative explanation is suggested by visual examination of a Schmidt plate taken by one of us (DW) in the region of RS Pup. The image reveals a number of near-identical dust clumps, with similar angular sizes, in the vicinity of the RS Pup nebula. If these clumps are at the same physical distance and are physically related, but only one of them has a Cepheid in it, it could be argued that they are all likely pre-existing nebulae—that is, not the result of Cepheid mass loss. The counter-argument would be that the ring-like structures observed in the surrounding nebula appear to be centered on RS Pup (Havlen 1972): this would be an extreme coincidence if the nebula were unrelated to the star.

Before our *Spitzer* observations, only two Cepheids had unambiguous evidence for circumstellar nebulae: ℓ Car and RS Pup. We have now doubled that number with the addition of S Mus and δ Cep; if extended emission around GH Lup, T Mon and X Cyg is confirmed, this would increase the sample size even more. A rough estimate of the fraction of Cepheids with substantial dusty mass loss can be made as 4 to 7 of 29, or $\sim 14 - 24\%$.⁴ The true fraction of Cepheids with mass loss could be below this limit if the observed nebulosity is related to the gas and dust from which the star formed. This is however unlikely, because even for small space velocities ($\sim 1 \text{ km s}^{-1}$, an order of magnitude less than the observed velocity of δ Cep and ℓ Car), in 50 Myr (the time it takes for an intermediate mass star to become a Cepheid) these stars will have moved away from their birthplace by several tens of parsecs. This is much larger than the size of the observed nebulosity around the stars in our sample.

Addressing the initial motivation for this study, it appears that mass loss, at least its dusty component visible in the infrared, can only partially account for the Cepheid mass loss discrepancy (e.g. up to 1/5th of a 10% discrepancy in the case of δ Cep, see Marengo et al. 2010b). Our estimates of Cepheid mass loss (in the range 10^{-8} to $10^{-9} M_{\odot} \text{ yr}^{-1}$) are comparable to previous studies based on the detection of infrared and UV excess (e.g. Welch & Duric

⁴The shells detected in the near-infrared around some Cepheids (Mérand et al. 2006, 2007; Kervella et al. 2006) are not consistent with dusty mass loss: they are very close to the stars and thus well above the dust sublimation temperature (Marengo et al. 2010a).

1988; Deasy 1988), but the higher spatial resolution of our images helps to separate local emission from background contamination. The detection of shocked structures, as in the case of δ Cep and possibly ℓ Car, is a compelling indication of current mass loss in those stars. While the total mass lost over the Cepheid phase is small, the confirmation that these processes are active needs to be taken into account for a proper modeling of Cepheid evolution. The presence of significant Cepheid winds can affect hydrodynamic models of Cepheid pulsations, and the way shock waves propagate in the Cepheid atmospheres. Finally, the observed level of circumstellar dust needs to be further explored, as it may have a significant effect on inferred Cepheid distances as shown by Neilson et al. (2010).

The authors thank H. Neilson for useful conversations and L.D. Matthews for assistance with computing the projected space velocity of ℓ Car. We thank the referee for helpful comments. This work is based on observations made with the *Spitzer Space Telescope*, which is operated by the Jet Propulsion Laboratory, California Institute of Technology under NASA contract 1407. Support for this work was provided by NASA through an award issued by JPL/Caltech. PB and DLW acknowledge research support through Discovery Grants from the Natural Sciences and Engineering Research Council of Canada; PB also acknowledges support from an Ontario Early Researcher Award. NRE acknowledges support from the Chandra X-Ray Center grant NAS8-03060. DH was supported in part by the National Science Foundation REU and Department of Defense ASSURE programs under Grant no. 0754568 and by the Smithsonian Institution.

Facilities: Spitzer (IRAC, MIPS).

REFERENCES

- Andrievsky, S. M., Luck, R. E., & Kovtyukh, V. V. 2005, *AJ*, 130, 1880
- Benedict, G. F. et al. 2007, *AJ*, 133, 1810
- Bono, G., Caputo, F., Cassisi, S., Marconi, M., Piersanti, L., & Tornambè, A. 2000, *ApJ*, 543, 955
- Bono, G., Caputo, F., & Castellani, V. 2006, *Memorie della Societa Astronomica Italiana*, 77, 207
- Bono, G., Gieren, W. P., Marconi, M., Fouqué, P., & Caputo, F. 2001, *ApJ*, 563, 319
- Caputo, F., Bono, G., Fiorentino, G., Marconi, M., & Musella, I. 2005, *ApJ*, 629, 1021

- Cardelli, J. A., Clayton, G. C., & Mathis, J. S. 1989, *ApJ*, 345, 245
- Christy, R. F. 1968, *QJRAS*, 9, 13
- Deasy, H. P. 1988, *MNRAS*, 231, 673
- Evans, A., Stickel, M., van Loon, J. T., Eyres, S. P. S., Hopwood, M. E. L., & Penny, A. J. 2003, *A&A*, 408, L9
- Evans, N. R. 1992, *ApJ*, 384, 220
- Evans, N. R., Carpenter, K., Robinson, R., Massa, D., Wahlgren, G. M., Vinko, J. & Szabados, L. 1999, *ApJ*, 524, 379
- Evans, N. R., Massa, D., Fullerton, A., Sonneborn, G., & Iping, R. 2006, *ApJ*, 647, 1387
- Evans, N. R., Massa, D., & Proffitt, C. 2009, *AJ*, 137, 3700
- Evans, N. R., Schaefer, G. H., Bond, H. E., Bono, G., Karovska, M., Nelan, E., Sasselov, D., & Mason, B. D. 2008, *AJ*, 136, 1137
- Fazio, G. G. et al. 2004, *ApJS*, 154, 10
- Fernie, J. D., Evans, N. R., Beattie, B., & Seager, S. 1995, *Information Bulletin on Variable Stars*, 4148, 1
- Fouqué, P. et al. 2007, *A&A*, 476, 73
- Frayer, D. T. et al. 2006, *AJ*, 131, 250
- Freedman, W. L., Madore, B. F., Rigby, J., Persson, S. E., & Sturch, L. 2008, *ApJ*, 679, 71
- Fricke, K., Stobie, R. S., & Strittmatter, P. A. 1972, *ApJ*, 171, 593
- Gehrz, R. D. 1972, *ApJ*, 178, 715
- Gieren, W. P., Fouque, P., & Gomez, M. I. 1997, *ApJ*, 488, 74
- Groenewegen, M. A. T. 2008, *A&A*, 488, 25
- Hainline, L. J., Blain, A. W., Smail, I., Frayer, D. T., Chapman, S. C., Ivison, R. J., & Alexander, D. M. 2009, *ApJ*, 699, 1610
- Havlen, R. J. 1972, *A&A*, 16, 252
- Helou, G. & Walker, D. W. 1988, in *NASA RP-1190*, Vol. 7 (1988)

- Hodge, T. M., Kraemer, K. E., Price, S. D., & Walker, H. J. 2004, *ApJS*, 151, 299
- Hora, J. L. et al. 2008, *AJ*, 135, 726
- Jones, T. W. & Merrill, K. M. 1976, *ApJ*, 209, 509
- Keller, S. C. 2008, *ApJ*, 677, 483
- Keller, S. C. & Wood, P. R. 2006, *ApJ*, 642, 834
- Kervella, P., Mérand, A., & Gallenne, A. 2009, *A&A*, 498, 425
- Kervella, P., Mérand, A., Perrin, G., & Coudé Du Foresto, V. 2006, *A&A*, 448, 623
- Kervella, P., Mérand, A., Szabados, L., Fouqué, P., Bersier, D., Pompei, E., & Perrin, G. 2008, *A&A*, 480, 167
- Kirk, J. M. et al. 2009, *ApJS*, 185, 198
- Koen, C., Marang, F., Kilkenny, D., & Jacobs, C. 2007, *MNRAS*, 380, 1433
- Kovtyukh, V. V., Andrievsky, S. M., Belik, S. I., & Luck, R. E. 2005, *AJ*, 129, 433
- Krist, J. E. 2006, *Spitzer Tiny TIM Spitzer Tiny TIM User's Guide Version 2.0* (Pasadena, CA: Caltech)
- Laney, C. D. & Stobie, R. S. 1994, *MNRAS*, 266, 441
- Luhman, K. L. et al. 2007, *ApJ*, 654, 570
- Marengo, M., Evans, N. R., Barmby, P., Bono, G., Welch, D. L., & Romaniello, M. 2010a, *ApJ*, 709, 120
- Marengo, M., Megeath, S. T., Fazio, G. G., Stapelfeldt, K. R., Werner, M. W., & Backman, D. E. 2006, *ApJ*, 647, 1437
- Marengo, M. et al. 2010b, *ApJ*, in press
- McAlary, C. W. & Welch, D. L. 1986, *AJ*, 91, 1209
- Mérand, A. et al. 2006, *A&A*, 453, 155
- . 2007, *ApJ*, 664, 1093
- Moskalik, P., Buchler, J. R., & Marom, A. 1992, *ApJ*, 385, 685

- Muñoz-Mateos, J. C. et al. 2009, *ApJ*, 703, 1569
- Nardetto, N., Gieren, W., Kervella, P., Fouqué, P., Storm, J., Pietrzynski, G., Mourard, D. & Queloz, D. 2009, *A&A*, 502, 951
- Neilson, H. R. & Lester, J. B. 2008, *ApJ*, 684, 569
- Neilson, H. R., Ngeow, C., Kanbur, S. M., & Lester, J. B. 2010, *ApJ*, 716, 1136
- Neilson, H. R., Ngeow, C.-C., Kanbur, S. M., & Lester, J. B. 2009, *ApJ*, 692, 81
- Ngeow, C. & Kanbur, S. M. 2008, *ApJ*, 679, 76
- Noriega-Crespo, A., van Buren, D., Cao, Y., & Dgani, R. 1997, *AJ*, 114, 837
- Pedicelli, S. et al. 2010, *A&A*, 518, A11
- Persson, S. E., Madore, B. F., Krzemiński, W., Freedman, W. L., Roth, M., & Murphy, D. C. 2004, *AJ*, 128, 2239
- Perryman, M. A. C. et al. 1997, *A&A*, 323, L49
- Rieke, G. H. et al. 2004, *ApJS*, 154, 25
- Romaniello, M., Primas, F., Mottini, M., Pedicelli, S., Lemasle, B., Bono, G., François, P., Groenewegen, M. A. T., & Laney, C. D. 2008, *A&A*, 488, 731
- Schuster, M. T., Marengo, M., & Patten, B. M. 2006, in *Society of Photo-Optical Instrumentation Engineers (SPIE) Conference Series*, Vol. 6270
- Shupe, D. L. et al. 2008, *AJ*, 135, 1050
- Stobie, R. S. 1969, *MNRAS*, 144, 511
- Su, K. Y. L., Rieke, G. H., Stapelfeldt, K. R., Smith, P. S., Bryden, G., Chen, C. H., & Trilling, D. E. 2008, *ApJ*, 679, L125
- Turner, D. G. 1992, *AJ*, 104, 1865
- Vink, J. S. 2008, *New Astronomy Review*, 52, 419
- Welch, D. L. & Duric, N. 1988, *AJ*, 95, 1794
- Werner, M. W. et al. 2004, *ApJS*, 154, 1
- Westerlund, B. 1961, *PASP*, 73, 72

Willson, L. A., Struck, C., Wang, Q., & Kawaler, S. D. 2008, *Physica Scripta* Volume T, 133, 014008

Table 1. Surface photometry of extended infrared emission

Star/region	5.8 μm	8 μm	24 μm	70 μm
GH Lup 1	0.07 ± 0.01	0.27 ± 0.01	0.16 ± 0.02	1.1 ± 0.1
GH Lup 2	0.02 ± 0.01	0.36 ± 0.01	0.29 ± 0.02	1.8 ± 0.1
GH Lup 3	0.13 ± 0.01	0.49 ± 0.01	0.51 ± 0.02	3.5 ± 0.2
GH Lup 4	0.10 ± 0.01	0.41 ± 0.01	0.46 ± 0.02	2.6 ± 0.1
RS Pup 1	0.24 ± 0.03	0.63 ± 0.02	0.89 ± 0.39	9.4 ± 0.8
RS Pup 2	0.18 ± 0.01	0.56 ± 0.01	0.82 ± 0.30	24 ± 1
RS Pup 3	0.27 ± 0.01	0.83 ± 0.03	1.99 ± 0.86	40 ± 1
RS Pup 4	0.33 ± 0.01	0.91 ± 0.01	3.10 ± 0.72	47 ± 1
RS Pup 5	0.23 ± 0.01	0.84 ± 0.03	3.14 ± 2.08	35 ± 2
S Mus 1 ^a	0.05 ± 0.01	0.10 ± 0.01	1.3 ± 1.1	2.0 ± 0.2
S Mus 2	0.08 ± 0.01	0.09 ± 0.01	0.8 ± 0.6	1.9 ± 0.1
S Mus 3	0.15 ± 0.01	0.16 ± 0.01	0.7 ± 0.3	0.9 ± 0.1
S Mus 4	0.07 ± 0.01	0.11 ± 0.01		

^aFor S Mus, regions are not the same in IRAC and MIPS.

Note. — All surface brightness values in MJy sr⁻¹.

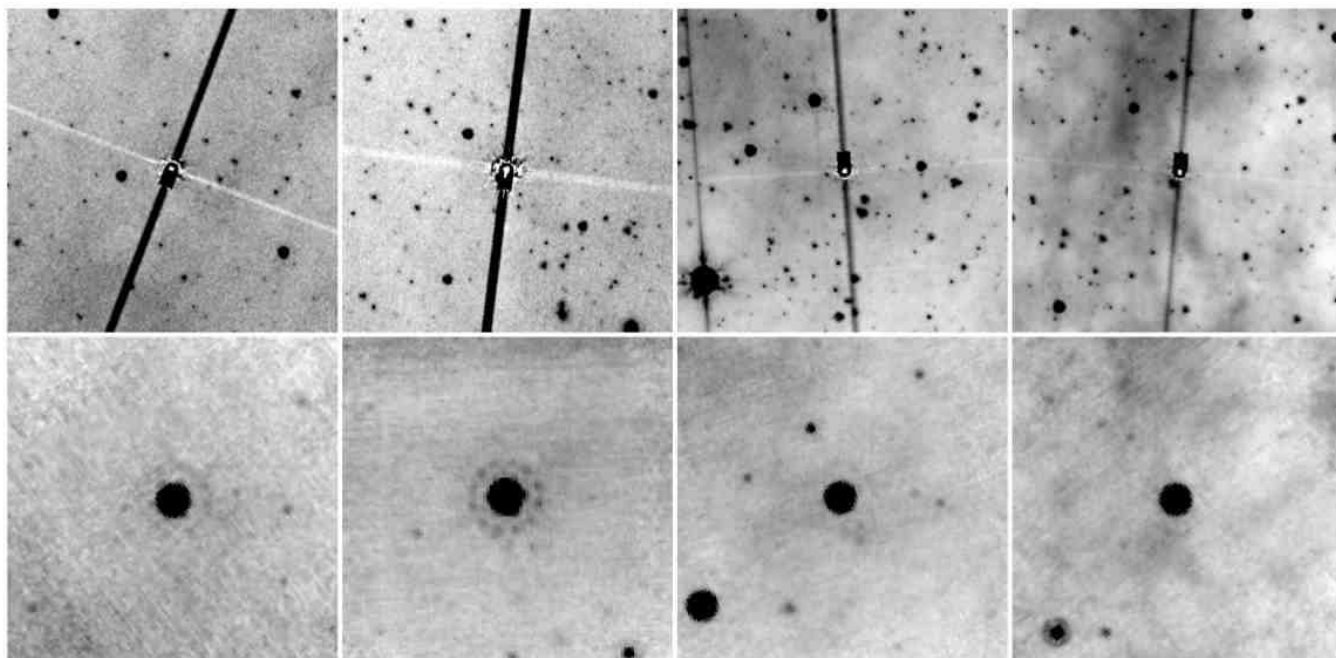


Fig. 1.— Images of some Cepheids with nearby extended infrared emission unrelated to the star. Left to right: DT Cyg, FF Aql, V Cen, and VY Car. Top row: PSF-subtracted IRAC 8.0 μm images, Bottom row: non-subtracted MIPS 24 μm images. All fields of view are 4 arcminute squares. In these and all following images, north is oriented up and east left. The black and white bands in the IRAC images are artifacts from both the bright source and the PSF-subtraction process.

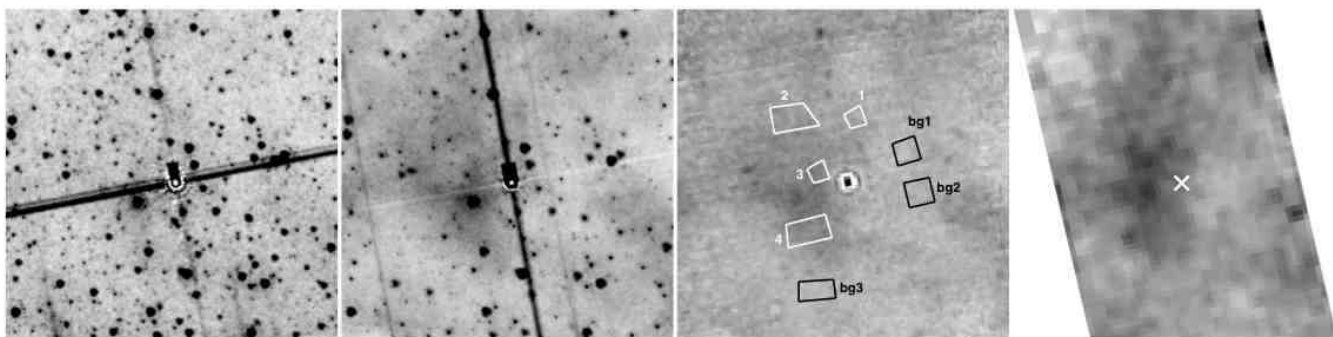


Fig. 2.— PSF-subtracted images of GH Lup in the (left to right) 5.8 μm and 8.0 μm IRAC bands, and the 24 μm and 70 μm (not PSF-subtracted; the white X marks the position of the star) MIPS bands. The field of view is a 4 arcminute square. Numbered boxes are regions used for surface photometry (see §2.2).

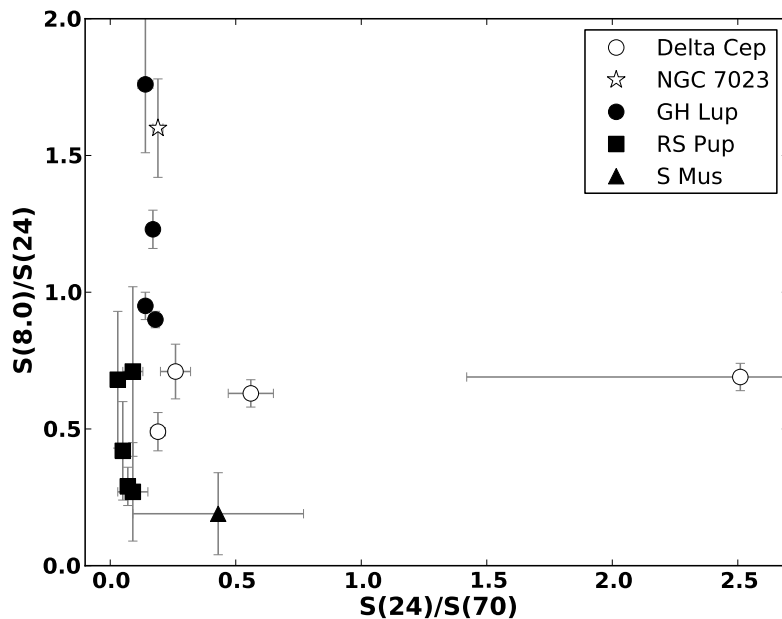


Fig. 3.— Left: Surface brightness ratios of extended emission near GH Lup, RS Pup and S Mus, with emission near δ Cep (circles) and NGC 7023 (star) shown for comparison. Increasing values on the horizontal axis correspond roughly to increasing dust temperature, while increasing values on the vertical axis correspond to increasing PAH content.

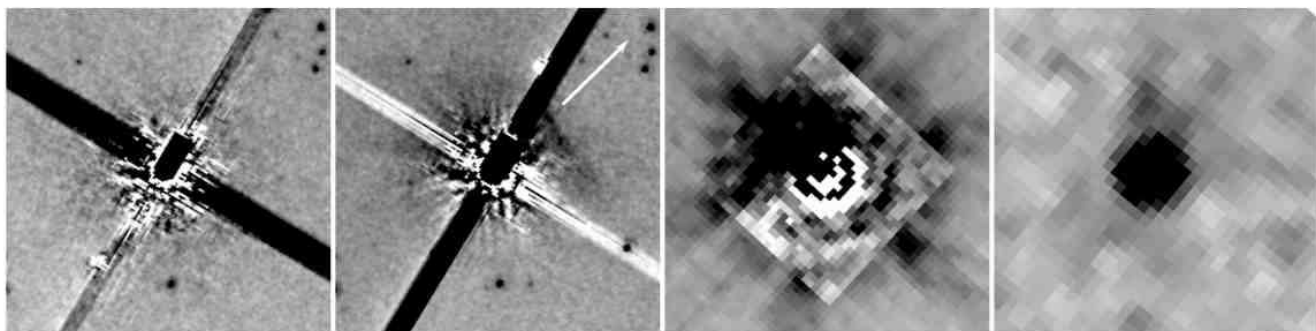


Fig. 4.— PSF-subtracted images of ℓ Car in the (left to right) 5.8 μm and 8.0 μm IRAC bands, and the 24 μm and 70 μm (not PSF-subtracted) MIPS bands. The field of view is a 2 arcminute square. The white arrow in the second panel shows the direction of the star's proper motion relative to the local ISM.

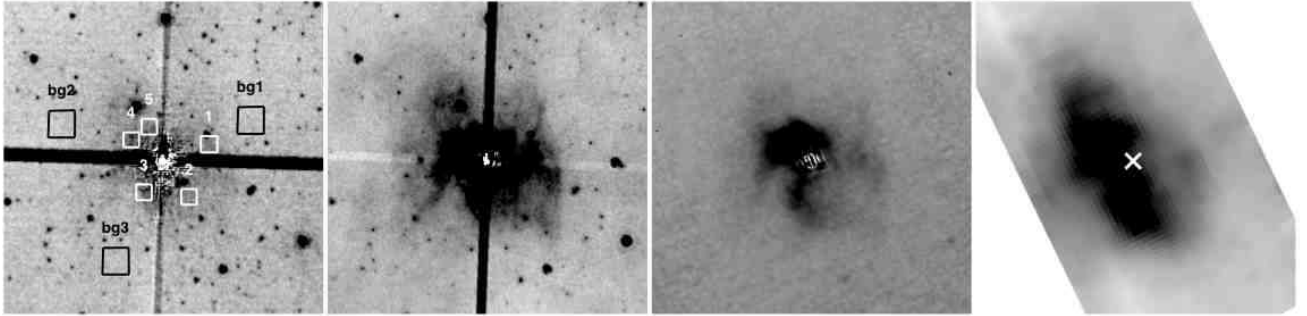


Fig. 5.— PSF-subtracted images of the reflection nebula around RS Pup in the (left to right) $5.8 \mu\text{m}$ and $8.0 \mu\text{m}$ IRAC bands, and the $24 \mu\text{m}$ and $70 \mu\text{m}$ MIPS bands (not PSF-subtracted; the white X marks the position of the star). The field of view is a 4 arcminute square. Numbered boxes are regions used for surface photometry (see §2.2).

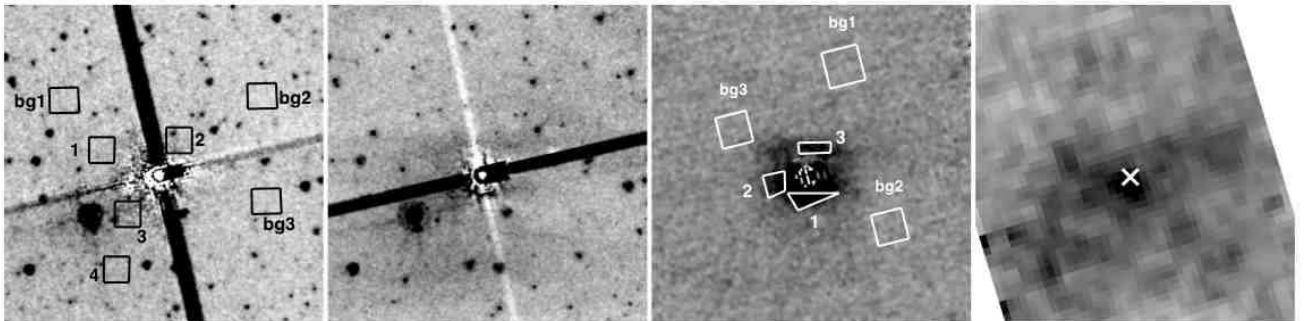


Fig. 6.— PSF-subtracted images of S Mus in the (left to right) $5.8 \mu\text{m}$ and $8.0 \mu\text{m}$ IRAC bands, and the $24 \mu\text{m}$ and $70 \mu\text{m}$ (not PSF-subtracted) MIPS bands; the white X marks the position of the star. The field of view is a 3 arcminute square. Numbered boxes are regions used for surface photometry (see §2.2).

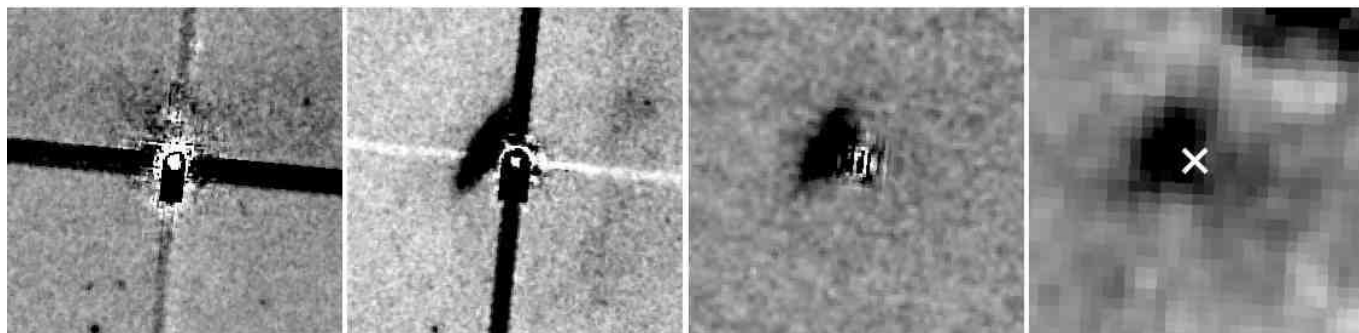


Fig. 7.— PSF-subtracted images of SZ Tau in the (left to right) $5.8 \mu\text{m}$ and $8.0 \mu\text{m}$ IRAC bands, and the $24 \mu\text{m}$ and $70 \mu\text{m}$ (not PSF-subtracted) MIPS bands; the white X marks the position of the star. The field of view is a 2 arcminute square. Of particular interest is the elongated object to the northeast of the star.

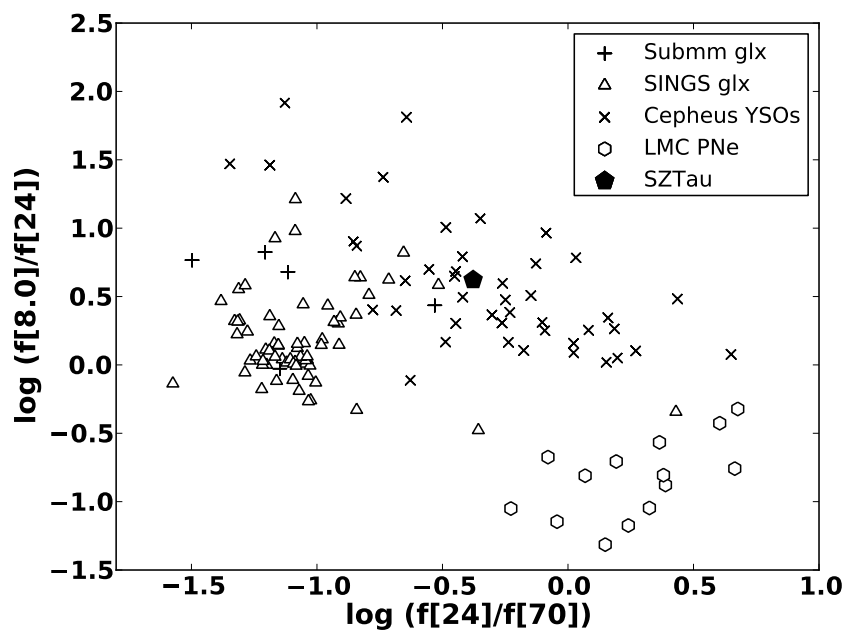


Fig. 8.— Right: flux density ratios for submillimeter-detected galaxies (Hainline et al. 2009), nearby galaxies (Muñoz-Mateos et al. 2009), Cepheus young stellar objects (Kirk et al. 2009), LMC planetary nebulae (Hora et al. 2008), and the extended emission near SZ Tau.

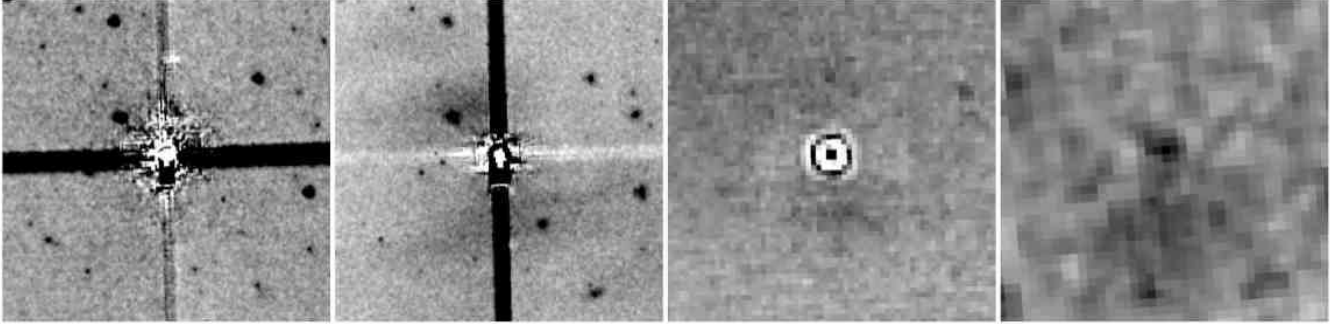


Fig. 9.— PSF-subtracted images of T Mon, in the (left to right) $5.8 \mu\text{m}$ and $8.0 \mu\text{m}$ IRAC bands, and the $24 \mu\text{m}$ and $70 \mu\text{m}$ (not PSF-subtracted) MIPS bands, All images are 2.5 arcminutes square.

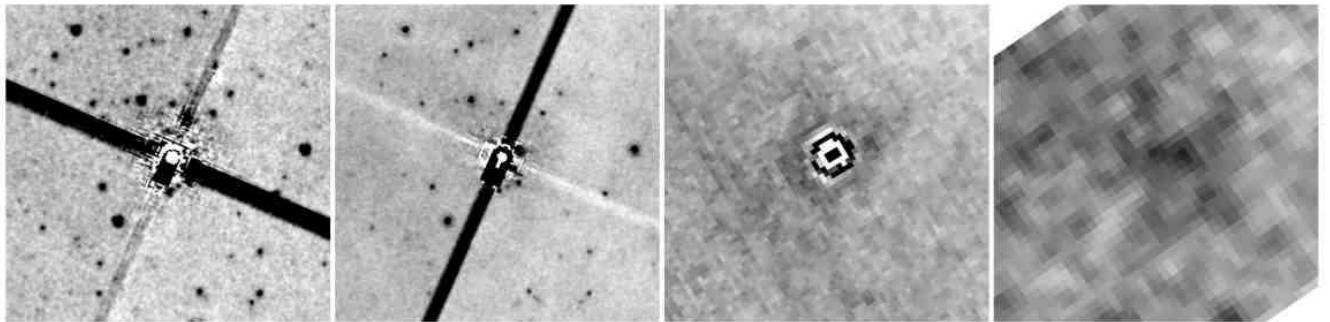


Fig. 10.— PSF-subtracted images of X Cyg in the (left to right) $5.8 \mu\text{m}$ and $8.0 \mu\text{m}$ IRAC bands, and the $24 \mu\text{m}$ and $70 \mu\text{m}$ (not PSF-subtracted) MIPS bands. The field of view is a 2.5 arcminute square.